Theoretical study of the He–HF^+ complex. II. Rovibronic states from coupled diabatic potential energy surfaces

G. Dhont
Groupe de Chimie Théorique, Université de Marne-la-Vallée, F-77454 Champs sur Marne, France

W. B. Zeimen, G. C. Groenenboom, and A. van der Avoird[a)]
Institute of Theoretical Chemistry, NSRIM, University of Nijmegen, Toernooiveld 1, 6525 ED Nijmegen, The Netherlands

(Received 26 August 2003; accepted 6 October 2003)

The bound rovibronic levels of the He–HF^+ complex were calculated for total angular momentum $J=\frac{1}{2}$, $\frac{3}{2}$, $\frac{5}{2}$, $\frac{7}{2}$, and $\frac{9}{2}$ with the use of *ab initio* diabatic intermolecular potentials presented in Paper I and the inclusion of spin–orbit coupling. The character of the rovibronic states was interpreted by a series of calculations with the intermolecular distance R fixed at values ranging from 1.5 to 8.5 Å and by analysis of the wave functions. In this analysis we used approximate angular momentum quantum numbers defined with respect to a dimer body-fixed (BF) frame with its z axis parallel to the intermolecular vector **R** and with respect to a molecule-fixed (MF) frame with its z axis parallel to the HF^+ bond. The linear equilibrium geometry makes the He–HF^+ complex a Renner–Teller system. We found both sets of quantum numbers, BF and MF, useful to understand the characteristics of the Renner–Teller effect in this system. In addition to the properties of a ''normal'' semirigid molecule Renner–Teller system it shows typical features caused by large-amplitude internal (bending) motion. We also present spectroscopic data: stretch and bend frequencies, spin–orbit splittings, parity splittings, and rotational constants. © *2004 American Institute of Physics.* [DOI: 10.1063/1.1629672]

I. INTRODUCTION

The preceding paper,[1] from now on referred to as Paper I, presents the calculation of the two asymptotically degenerate adiabatic potential surfaces of the He–HF^+ complex that correlate with the degenerate $X\,^2\Pi$ ground state of HF^+. The twofold spatial degeneracy of this Π state is lifted, except when the complex has a linear geometry. The method used for this calculation is a recently proposed[2] *ab initio* method that combines the potential energy surface of the neutral closed-shell complex, He–HF in this case, with the ionization energies of the complex and of one of the monomers (here HF) to obtain the interaction energy of the cationic complex. Multiple (excited state) potential surfaces can be efficiently generated by the computation of higher ionization energies of the neutral species, a feature that is used in this case to obtain simultaneously the lowest two asymptotically degenerate potential surfaces of He–HF^+. Paper I also presents diabatic surfaces obtained from the two adiabatic ones and a full analytic fit of these diabatic surfaces. In the present paper we proceed by calculating the rovibronic states of the complex on the diabatic potential surfaces, with the inclusion of spin–orbit coupling. In Sec. II we describe the formalism used to perform these calculations in space-fixed and different body-fixed coordinates. The nonadiabatic coupling that is particularly important near the linear geometry of the complex where the adiabatic states become degenerate is implicitly taken into account in these calculations. In Sec. III we present and discuss the results, first of one-dimensional calculations with the intermolecular distance R fixed at a range of values, then of the full calculations.

Since the two potential surfaces computed in Paper I correspond to a linear equilibrium geometry of He–HF^+ this complex is a Renner–Teller system. It is much more strongly bound than the neutral Van der Waals complex He–HF, but considerably less rigid than a normal, chemically bound, linear triatomic molecule where Renner–Teller coupling has mostly been studied. Therefore, we will pay special attention, in Sec. III C, to the way in which the Renner–Teller effect becomes manifest in this system. We will compare our results to those of Schmelz and Rosmus,[3] who made a similar study on different potential surfaces.

II. CALCULATION OF ROVIBRONIC STATES

Different coordinates and basis sets can be used to calculate the vibration–rotation–tunneling levels of Van der Waals dimers. In particular, one may choose a space-fixed (SF) basis or various body-fixed (BF) bases,[4,5] as well as different angular momentum coupling schemes.[6] The rovibronic states of He–HF^+ were first calculated in this work in a coupled SF basis. For the interpretation of the results and the understanding of the Renner–Teller effect it turned out, however, that the expansion of the rovibronic states and the consideration of various approximate quantum numbers with respect to different BF frames was very useful. So, we also performed calculations with body-fixed bases with angular momentum projection quantum numbers defined either BF with respect to the vector **R** that points from the HF^+ center

a)Author to whom correspondence should be addressed. Electronic mail: avda@theochem.kun.nl

of mass to the He nucleus or molecule fixed (MF) with respect to the HF^+ bond axis **r**. It is not necessary to repeat the computation of the energy levels in the different frames; the transformation from the SF basis to the BF and MF bases is given analytically. Before we discuss the formalism to compute the rovibronic levels of the complex, we briefly summarize the fine structure of HF^+ in its $X\,^2\Pi$ ground state.

The dominant term that splits the levels of $HF^+(X\,^2\Pi)$ is the spin–orbit coupling (coupling constant $A=-293.14\ \mathrm{cm}^{-1}$). Approximate quantum numbers that characterize these energy levels are $\Lambda=\pm 1$ and $\Omega=\Lambda+\Sigma$. The quantum number Λ is the eigenvalue of the electronic orbital angular momentum operator $\hat{l}_z$ and $\Sigma=-\frac{1}{2},\frac{1}{2}$ is the eigenvalue of $\hat{S}_z$, which is the component of the spin ($S=\frac{1}{2}$) along the HF^+ bond axis. The total angular momentum of the HF^+ monomer is represented by the operator $\hat{\mathbf{j}}=\hat{\mathbf{l}}+\hat{\mathbf{S}}+\hat{\mathbf{R}}$, where $\hat{\mathbf{l}}$, $\hat{\mathbf{S}}$, and $\hat{\mathbf{R}}$ are the electronic orbital and spin, and the nuclear (rotation) angular momenta, respectively. For free HF^+ the quantum number j that corresponds with the operator $\hat{\mathbf{j}}$ is an exact quantum number. The eigenvalue Ω of the electronic angular momentum operator $\hat{l}_z+\hat{S}_z$ is also an eigenvalue of $\hat{j}_z$, because the nuclear angular momentum $\hat{\mathbf{R}}$ has a vanishing z component. As a result of spin–orbit coupling, the levels with $\Omega=\pm\frac{3}{2}$ are lower by about 300 cm^{-1} than the levels with $\Omega=\pm\frac{1}{2}$, which makes $HF^+(X\,^2\Pi)$ a typical Hund's coupling case (a) system. For $j>0$ Ω is not an exact quantum number even for the free monomer, because states with different Ω are slightly mixed by Coriolis coupling. The effective monomer Hamiltonian that describes the complete level structure of $HF^+(X\,^2\Pi)$ is

$$\hat{H}_{HF^+}=B_0[\hat{j}^2+\hat{S}^2-\hat{j}_z^2-\hat{S}_z^2-\hat{S}_-\hat{j}_--\hat{S}_+\hat{j}_+]+A\,\hat{l}_z\hat{S}_z, \qquad (1)$$

where $B_0=17.5779\ \mathrm{cm}^{-1}$ is the rotational constant and $A=-293.14\ \mathrm{cm}^{-1}$ the spin–orbit coupling constant of $HF^+(X\,^2\Pi)$ in its vibrational ground state.[7] The components of the angular momentum operator $\hat{\mathbf{j}}$ are given with respect to the MF z axis and obey anomalous commutation relations.[8] The corresponding shift operators are therefore defined as $\hat{j}_\pm=\hat{j}_x\mp i\hat{j}_y$, whereas the spin shift operators have the normal definition $\hat{S}_\pm=\hat{S}_x\pm i\hat{S}_y$.

Since the H–F vibration has a much higher frequency than the vibrations of the He–HF^+ complex we froze the HF^+ bond length at the equilibrium value $r_e=1.0011$ Å.[7] It was shown in Paper I that the intermolecular potential depends strongly on the HF^+ bond length, however. The global minimum in a full three-dimensional potential, which is the sum of the intermolecular potential and the H–F^+ pair potential, occurs at $r=1.0273$ Å. We also computed rovibronic levels with r fixed at this value. The Hamiltonian of the He–$HF^+(X\,^2\Pi)$ complex in SF coordinates can then be written (in atomic units) as

$$\hat{H}=\frac{-1}{2\mu R}\frac{\partial^2}{\partial R^2}R+\frac{\hat{L}^2}{2\mu R^2}+\hat{H}_{HF^+}+\hat{V}, \qquad (2)$$

where $\mu=3.3353$ u is the reduced mass of the dimer and $\hat{\mathbf{L}}$ is the angular momentum operator corresponding to the end-over-end rotation. The potential energy operator $\hat{V}$, given in terms of diabatic states, is most conveniently expressed in body-fixed coordinates and will be specified below. In writing Eq. (2) we assumed implicitly that the interaction with He does not change the spin–orbit coupling term in the Hamiltonian of the HF^+ monomer. The SF dimer basis and the matrix elements of the Hamiltonian in Eqs. (1) and (2) over this basis can be found in a recent paper on the bound levels of the He–$CO(a\,^3\Pi)$ complex.[9]

A. R embedding

Since He–$HF^+(X\,^2\Pi)$ is much more strongly bound than He–$CO(a\,^3\Pi)$ the bound states of He–$HF^+(X\,^2\Pi)$ are most conveniently calculated and interpreted in a basis with coordinates and angular momentum quantum numbers defined with respect to a BF frame with its z axis along **R**. The BF coordinates are defined by writing the SF components of the vectors **R** and **r** as

$$\mathbf{R}=R\mathbb{R}_z(\alpha)\mathbb{R}_y(\beta)\mathbf{e}_z, \qquad (3)$$

$$\mathbf{r}=r\mathbb{R}_z(\alpha)\mathbb{R}_y(\beta)\mathbb{R}_z(\phi)\mathbb{R}_y(\theta)\mathbf{e}_z \qquad (4)$$

with the unit vector $\mathbf{e}_z$ being the column vector (0,0,1) and the rotation matrices

$$\mathbb{R}_z(\alpha)=\begin{pmatrix}\cos\alpha & -\sin\alpha & 0\\ \sin\alpha & \cos\alpha & 0\\ 0 & 0 & 1\end{pmatrix},$$

$$\mathbb{R}_y(\beta)=\begin{pmatrix}\cos\beta & 0 & \sin\beta\\ 0 & 1 & 0\\ -\sin\beta & 0 & \cos\beta\end{pmatrix}. \qquad (5)$$

The BF coordinate θ is the angle between **r** and **R** which is zero for the linear He–HF^+ geometry. The elements of the matrix $\mathbb{R}(\alpha,\beta,\phi)=\mathbb{R}_z(\alpha)\mathbb{R}_y(\beta)\mathbb{R}_z(\phi)$ are the direction cosines of the (three-angle embedded) BF frame with respect to the SF frame.

The Hamiltonian for the rovibronic states of the complex on the multiple diabatic potential surfaces reads in BF coordinates as

$$\hat{H}=\frac{-1}{2\mu R}\frac{\partial^2}{\partial R^2}R+\frac{\hat{j}^2-2\hat{\mathbf{j}}\cdot\hat{\mathbf{J}}+\hat{J}^2}{2\mu R^2}+\hat{H}_{HF^+}+\sum_{\Lambda',\Lambda}|\Lambda'\rangle^{BF}V^{BF}_{\Lambda',\Lambda}(R,\theta)^{BF}\langle\Lambda|. \qquad (6)$$

The monomer Hamiltonian $\hat{H}_{HF^+}$ is the same as in the SF representation, see Eq. (1). The diabatic states $|\Lambda\rangle^{BF}$ of the He–$HF^+(X\,^2\Pi)$ complex, labeled by the HF^+ monomer quantum number $\Lambda=\pm 1$, are here expressed in BF coordinates, cf. Eq. (A8). The expansion of the diabatic potentials is given by

$$V^{\mathrm{BF}}_{\Lambda',\Lambda}(R,\theta) = {}^{\mathrm{BF}}\langle\Lambda'|\hat{V}|\Lambda\rangle^{\mathrm{BF}} = \sum_l v_l^{\Lambda',\Lambda}(R) D^{(l)}_{0,\Lambda-\Lambda'}(0,\theta,0). \quad (7)$$

The functions $D^{(l)}_{m',m}(\phi,\theta,\chi)$ are Wigner rotation functions[8] with two of the angles being zero in this case; note that only functions with $m'=0$ and $m=\Lambda-\Lambda'$ occur in the expansion. We obtained the above expansion from the corresponding expansion in MF coordinates derived in Ref. 9

$$V^{\mathrm{MF}}_{\Lambda',\Lambda}(R,\theta) = \sum_l v_l^{\Lambda',\Lambda}(R) D^{(l)}_{\Lambda-\Lambda',0}(0,\theta,0) = \sum_l v_l^{\Lambda',\Lambda}(R) C^{(l)}_{\Lambda-\Lambda'}(\theta,0) \quad (8)$$

with the use of the transformation of the electronic wave functions in Eq. (A9). The functions $C^{(l)}_m(\theta,\phi)$ are Racah normalized spherical harmonics. It was demonstrated in Ref. 9 that the restriction of the expansion to functions with $m=\Lambda-\Lambda'$ follows from the invariance of the potential energy operator $\hat{V}$ under rotations of the complex about the HF$^+$ bond axis. The expansion coefficients $v_l^{\Lambda',\Lambda}(R)$ can be written, apart from a known normalization constant, as integrals over the diabatic potentials $V^{\mathrm{MF}}_{\Lambda',\Lambda}(R,\theta)$ multiplied with the corresponding spherical harmonic $C^{(l)}_{\Lambda-\Lambda'}(\theta,0)$. The integration over θ is performed with the analytic fits of the *ab initio* potentials from Paper I and the use of numerical Gauss–Legendre quadrature.

The BF dimer basis, as derived in Appendix A, reads

$$|n,\Lambda,S,\Omega,j,P_R;J,M_J\rangle = |n\rangle|\Lambda,S,\Omega\rangle^{\mathrm{BF}} \frac{[(2j+1)(2J+1)]^{1/2}}{4\pi} D^{(j)}_{P_R,\Omega}(0,\theta,0)^* \times D^{(J)}_{M_J,P_R}(\alpha,\beta,\phi)^*, \quad (9)$$

where the total angular momentum J and its SF z component M_J are exact quantum numbers and P_R is the projection of both **J** and the monomer angular momentum **j** on the BF z axis. The electronic wave function $|\Lambda,S,\Omega\rangle^{\mathrm{BF}}$, labeled by the Hund's case (a) quantum numbers Λ, S, Ω of HF$^+$, and implicitly by $\Sigma=\Omega-\Lambda$, is a diabatic wave function of the He–HF$^+$($X\,^2\Pi$) complex, here expressed in BF coordinates [Eq. (A8)]. The symmetric rotor function $D^{(j)}_{P_R,\Omega}(0,\theta,0)^*$ describes the HF$^+$ rotation with respect to the dimer BF frame and the function $D^{(J)}_{M_J,P_R}(\alpha,\beta,\phi)^*$ the overall rotation of the complex. The radial basis functions $|n\rangle=\chi_n(R)$ are Morse oscillator type functions of the form defined in Ref. 10.

The matrix elements of the Hamiltonian in the BF basis are

$$\begin{aligned}
&\langle n',\Lambda',S,\Omega',j',P'_R;J,M_J|\hat{H}|n,\Lambda,S,\Omega,j,P_R;J,M_J\rangle \\
&= \delta_{\Lambda',\Lambda}\delta_{\Omega',\Omega}\delta_{j',j}\delta_{P'_R,P_R}\Big[\langle n'|\frac{-1}{2\mu R}\frac{\partial^2}{\partial R^2}R|n\rangle + \langle n'|\frac{1}{2\mu R^2}|n\rangle(J(J+1)+j(j+1)-2P_R^2) + \delta_{n',n}B_0(j(j+1)+S(S+1) \\
&\quad -\Omega^2-\Sigma^2) + \delta_{n',n}A\Lambda\Sigma\Big] - \delta_{j',j}\delta_{\Lambda',\Lambda}\Big[\delta_{\Omega',\Omega}\langle n'|\frac{1}{2\mu R^2}|n\rangle(C^J_{P'_R,P_R-1}C^j_{P'_R,P_R-1} + C^J_{P'_R,P_R+1}C^j_{P'_R,P_R+1}) \\
&\quad + B_0\delta_{P'_R,P_R}\delta_{n',n}(C^j_{\Omega',\Omega-1}C^S_{\Sigma',\Sigma-1} + C^j_{\Omega',\Omega+1}C^S_{\Sigma',\Sigma+1})\Big] + \langle n',\Lambda',S,\Omega',j',P'_R;J,M_J|\hat{V}|n,\Lambda,S,\Omega,j,P_R;J,M_J\rangle \quad (10)
\end{aligned}$$

with shift matrix elements $C^j_{m',m\pm1} = \delta_{m',m\pm1}\sqrt{j(j+1)-m(m\pm1)}$. The matrix elements of the potential energy operator are

$$\langle n',\Lambda',S,\Omega',j',P'_R;J,M_J|\hat{V}|n,\Lambda,S,\Omega,j,P_R;J,M_J\rangle = \sqrt{(2j'+1)(2j+1)}(-1)^{P'_R-\Omega'}\delta_{\Sigma',\Sigma}\sum_l \langle n'|v_l^{\Lambda',\Lambda}(R)|n\rangle \begin{pmatrix} j' & l & j \\ -P'_R & 0 & P_R \end{pmatrix}\begin{pmatrix} j' & l & j \\ -\Omega' & \Lambda'-\Lambda & \Omega \end{pmatrix}. \quad (11)$$

The expressions in large round brackets are $3j$ symbols.[11]

The parity-adapted basis in the BF embedding is

$$|n,|\Lambda|,S,\Omega,j,P_R;J,M_J,p\rangle = |n,\Lambda,S,\Omega,j,P_R;J,M_J\rangle + p(-1)^{J-S}|n,-\Lambda,S,-\Omega,j,-P_R;J,M_J\rangle \quad (12)$$

with p being the parity under inversion and $p(-1)^{J-S}$ the spectroscopic parity, e or f.

B. r embedding

In order to recognize the characteristic features of a Renner–Teller system it is also useful to express the rovibronic wave functions in coordinates defined with respect to a frame with its z axis parallel to the HF$^+$ monomer bond axis **r**. We call this frame MF. The MF coordinates are defined by writing the SF components of the vectors **r** and **R** as

$$\mathbf{r} = r\mathbb{R}_z(\phi')\mathbb{R}_y(\theta')\mathbf{e}_z, \quad (13)$$

$$\mathbf{R} = R\mathbb{R}_z(\phi')\mathbb{R}_y(\theta')\mathbb{R}_z(\alpha')\mathbb{R}_y(\beta')\mathbf{e}_z. \quad (14)$$

The MF coordinate β', the angle between the vectors **R** and **r**, is the same as the BF coordinate θ. The matrix $\mathbb{R}(\phi',\theta',\alpha')=\mathbb{R}_z(\phi')\mathbb{R}_y(\theta')\mathbb{R}_z(\alpha')$ contains the direction cosines of the (three-angle embedded) MF frame with respect to the SF frame.

The dimer Hamiltonian in the MF representation is similar to the SF Hamiltonian in Eq. (2) except for the appearance of the HF^+ monomer term. Since the quantum number j is not defined in the MF representation, we write the HF^+ monomer Hamiltonian as

$$\hat{H}_{HF^+}=B_0[\hat{J}^2+\hat{L}^2+\hat{S}^2-\hat{J}_z^2-\hat{L}_z^2-\hat{S}_z^2-(\hat{L}_-\hat{J}_-+\hat{L}_+\hat{J}_+) -(\hat{S}_-\hat{J}_-+\hat{S}_+\hat{J}_+)+(\hat{L}_+\hat{S}_-+\hat{L}_-\hat{S}_+)]+A\,\hat{l}_z\hat{S}_z. \tag{15}$$

The potential energy operator is now

$$\hat{V}=\sum_{\Lambda',\Lambda}|\Lambda'\rangle^{\mathrm{MF}}\,V^{\mathrm{MF}}_{\Lambda',\Lambda}(R,\beta')\,{}^{\mathrm{MF}}\langle\Lambda| \tag{16}$$

with diabatic states $|\Lambda\rangle^{\mathrm{MF}}$ in MF coordinates, cf. Eq. (A7). The expansion of the diabatic potentials $V^{\mathrm{MF}}_{\Lambda',\Lambda}(R,\beta')$ is given by Eq. (8) with $\theta=\beta'$. The dimer basis functions in MF coordinates are (cf. the Appendix)

$$|n,\Lambda,S,\Omega,L,\Omega_L,P_r;J,M_J\rangle =|n\rangle|\Lambda,S,\Omega\rangle^{\mathrm{MF}}Y_{L\Omega_L}(\beta',0) \times\left[\frac{2J+1}{4\pi}\right]^{1/2}D^{(J)}_{M_J,P_r}(\phi',\theta',\alpha')^*, \tag{17}$$

where Ω_L is the projection of the end-over-end angular momentum **L** on the HF^+ axis and $P_r=\Omega+\Omega_L$ is the projection of the total angular momentum **J** on the same axis. The diabatic electronic wave functions $|\Lambda,S,\Omega\rangle^{\mathrm{MF}}$ are defined with respect to the MF frame [Eq. (A7)]. In Renner–Teller systems it is customary to define also a quantum number K, the projection of the electronic and nuclear orbital angular momenta on the body-fixed z axis or, in other words, the eigenvalue of the total angular momentum operator $\hat{J}_z$ minus the eigenvalue of the spin operator $\hat{S}_z$. Here we define $K_r=\Lambda+\Omega_L=P_r-\Sigma$. The matrix elements of the Hamiltonian in the MF basis read

$$\begin{aligned}&\langle n',\Lambda',S,\Omega',L',\Omega_L',P_r';J,M_J|\hat{H}|n,\Lambda,S,\Omega,L,\Omega_L,P_r;J,M_J\rangle\\ &=\delta_{\Lambda',\Lambda}\delta_{\Omega',\Omega}\delta_{L',L}\delta_{\Omega_L',\Omega_L}\Big[\langle n'|\frac{-1}{2\mu R}\frac{\partial^2}{\partial R^2}R|n\rangle+\langle n'|\frac{L(L+1)}{2\mu R^2}|n\rangle+\delta_{n',n}B_0(J(J+1)+L(L+1)+S(S+1)\\ &\quad-P_r^2-\Omega_L^2-\Sigma^2)+\delta_{n',n}A\Lambda\Sigma\Big]-B_0\delta_{\Lambda',\Lambda}\delta_{L',L}\delta_{n',n}[(C^J_{P_r',P_r-1}C^L_{\Omega_L',\Omega_L-1}+C^J_{P_r',P_r+1}C^L_{\Omega_L',\Omega_L+1})\\ &\quad+(C^J_{P_r',P_r-1}C^S_{\Sigma',\Sigma-1}+C^J_{P_r',P_r+1}C^S_{\Sigma',\Sigma+1})-(C^L_{\Omega_L',\Omega_L+1}C^S_{\Sigma',\Sigma-1}+C^L_{\Omega_L',\Omega_L-1}C^S_{\Sigma',\Sigma+1})]\\ &\quad+\langle n',\Lambda',S,\Omega',L',\Omega_L',P_r';J,M_J|\hat{V}|n,\Lambda,S,\Omega,L,\Omega_L,P_r;J,M_J\rangle.\end{aligned} \tag{18}$$

The matrix elements of the potential are

$$\begin{aligned}&\langle n',\Lambda',S,\Omega',L',\Omega_L',P_r';J,M_J|\hat{V}|n,\Lambda,S,\Omega,L,\Omega_L,P_r;J,M_J\rangle\\ &=\sqrt{(2L'+1)(2L+1)}\,\delta_{\Sigma',\Sigma}\delta_{P_r',P_r}\sum_l\langle n'|v_l^{\Lambda',\Lambda}(R)|n\rangle(-1)^{\Omega_L'}\begin{pmatrix}L' & l & L\\ 0 & 0 & 0\end{pmatrix}\begin{pmatrix}L' & l & L\\ -\Omega_L' & \Lambda-\Lambda' & \Omega_L\end{pmatrix}.\end{aligned} \tag{19}$$

The parity-adapted basis in the MF embedding is

$$\begin{aligned}&|n,|\Lambda|,S,\Omega,L,\Omega_L,P_r;J,M_J,p\rangle\\ &=|n,\Lambda,S,\Omega,L,\Omega_L,P_r;J,M_J\rangle\\ &\quad+p(-1)^{J-S}|n,-\Lambda,S,-\Omega,L,-\Omega_L,-P_r;J,M_J\rangle.\end{aligned} \tag{20}$$

It is also useful to know how to transform the basis from one frame to another. This is derived in the Appendix.

C. Computational details

The bound states of the complex were obtained from a full diagonalization of the Hamiltonian matrix. We coded the construction of this matrix in the three different sets of coordinates for which the formulas are given above (SF, BF, MF) and used the basis transformations specified in the Appendix to check our codes. Calculations were performed for J up to $\frac{9}{2}$ inclusive. The levels were converged to within 10^{-4} cm^{-1} with an angular basis truncated at $j_{\max}=\frac{35}{2}$ and a radial basis with $n_{\max}=14$. Test calculations with $j_{\max}=\frac{41}{2}$ gave levels that did not deviate from the $j_{\max}=\frac{35}{2}$ results by more than 10^{-5} cm^{-1}. The nonlinear parameters R_e, D_e, and ω_e of the 15 radial basis functions $\chi_n(R)$ were optimized by energy minimizations with smaller values of $n_{\max}$. The final calculation was performed using $R_e=5.3\ a_0$, $D_e=620\ \mathrm{cm}^{-1}$, and $\omega_e=140\ \mathrm{cm}^{-1}$.

TABLE I. Rovibronic states for $J=\frac{3}{2}$ from calculations with R fixed. Energies E in the first row correspond to states of e spectroscopic parity, $\Delta E=E_f-E_e$ in the second row is the parity splitting. The other entries are populations (in percent) of basis functions in **R** embedding with approximate quantum numbers P_R, Ω.

		$R=2.26$ Å				$R=3.7$ Å			
E (cm^{-1})		−1302.3696	−1031.1954	−898.0328	−686.5220	−225.9358	−196.2161	−178.4279	−168.6719
ΔE (cm^{-1})		−0.000 01	−0.076 37	−0.930 72	0.781 91	−0.000 01	−0.032 64	0.032 86	0.000 22
P_R	Ω								
$\frac{1}{2}$	$\frac{1}{2}$	0.00	79.60	20.48	2.47	0.00	0.98	0.01	0.00
$-\frac{1}{2}$	$\frac{1}{2}$	0.00	0.04	1.65	37.37	0.00	0.00	0.94	0.01
$\frac{1}{2}$	$\frac{3}{2}$	0.03	20.10	77.59	1.21	0.14	98.30	0.57	0.00
$-\frac{1}{2}$	$\frac{3}{2}$	0.00	0.22	0.25	57.23	0.00	0.58	97.24	1.23
$\frac{3}{2}$	$\frac{1}{2}$	0.73	0.01	0.01	0.23	0.78	0.00	0.00	0.00
$-\frac{3}{2}$	$\frac{1}{2}$	0.04	0.00	0.00	0.13	0.00	0.00	0.01	0.90
$\frac{3}{2}$	$\frac{3}{2}$	99.20	0.02	0.03	1.28	99.08	0.14	0.00	0.00
$-\frac{3}{2}$	$\frac{3}{2}$	0.00	0.00	0.00	0.09	0.00	0.00	1.23	97.86

III. RESULTS

A. One-dimensional calculations

In order to understand how the states of the HF^+ monomer become perturbed and mixed by the interaction with the He atom it is interesting to start with calculations in which the intermolecular distance R is fixed and is reduced from infinity to its equilibrium value. We have performed such fixed-R calculations for a set of distances ranging from 1.5 to 8.5 Å, with a grid spacing of 0.0085 Å for $R<3.3$ Å and 0.15 Å for larger distances. An analysis of the wave functions for $R=2.26$ and 3.7 Å in the **R** embedded frame is presented in Table I for $J=\frac{3}{2}$ and Table II for $J=\frac{1}{2}$. The first observation one can make is that the quantum number P_R, the projection of **J** on the BF z axis **R**, is always a nearly good quantum number. The energies are plotted as functions of R in Fig. 1 for $P_R=\pm\frac{1}{2}$, $J=\frac{1}{2}$ and for $P_R=\pm\frac{3}{2}$, $J=\frac{3}{2}$. The picture exhibits different dissociation limits. The lowest three limits correspond to the $|\Omega|=\frac{3}{2}$ ground state of the HF^+ monomer, the first one at -114.2138 cm^{-1} to $j=\frac{3}{2}$, the second one to $j=\frac{5}{2}$, and the third one to $j=\frac{7}{2}$. The fourth asymptote corresponds to the excited spin–orbit state of HF^+ with $|\Omega|=\frac{1}{2}$ and $j=\frac{1}{2}$. We did not plot the energies with $P_R=\pm\frac{1}{2}$, $J=\frac{3}{2}$ because they only differ from the $P_R=\pm\frac{1}{2}$, $J=\frac{1}{2}$ energy curves by one quantum of overall rotation and on the scale of Fig. 1 would coincide with the latter curves. The corresponding eigenvectors are very similar, cf. Tables I and II. The lowest curve has a global minimum at -1302.37 cm^{-1} for $R=2.258$ Å and corresponds to $J=\frac{3}{2}$, $P_R=\pm\frac{3}{2}$, $\Omega=\pm\frac{3}{2}$, and e parity.

Figure 1 shows that first, from large R inwards to about 3.7 Å, the asymptotic levels of given j split into $2j+1$ levels with $P_R=-j,-j+1,\ldots,j$ by the anisotropic interaction with the He atom. Monomer states of given Ω that in free HF^+ are mixed only by Coriolis coupling, are now coupled also by the off-diagonal diabatic interaction potentials $V_{\pm1,\mp1}$, i.e., by the adiabatic "difference potential" $(V_{A''}-V_{A'})/2$. For smaller distances the interaction with He becomes stronger, the energy curves in Fig. 1 show (avoided) crossings, and the monomer spin–orbit states with different $|\Omega|$ start to mix. This is illustrated for $R=2.26$ Å in Table I. Only the lowest bound state, with $|\Omega|=\frac{3}{2}$, shows negligible mixing with states of $|\Omega|=\frac{1}{2}$, cf. also Fig. 1.

TABLE II. Rovibronic states for $J=\frac{1}{2}$ from calculations with R fixed. For explanations, see Table I.

		$R=2.26$ Å				$R=3.7$ Å			
E (cm^{-1})		−1034.044 81	−901.087 22	−689.1133	−586.5951	−197.2510	−179.4627	−109.4178	−100.6141
ΔE (cm^{-1})		−0.038 19	−0.465 44	0.405 33	−0.131 69	−0.016 41	0.016 62	−0.085 87	0.085 72
P_R	Ω								
$\frac{1}{2}$	$\frac{1}{2}$	79.56	20.62	2.52	7.56	0.99	0.00	2.15	0.03
$-\frac{1}{2}$	$\frac{1}{2}$	0.07	1.61	37.96	35.96	0.00	0.96	0.02	2.24
$\frac{1}{2}$	$\frac{3}{2}$	20.20	77.38	1.44	37.59	98.89	0.12	96.82	1.01
$-\frac{1}{2}$	$\frac{3}{2}$	0.17	0.39	58.08	18.89	0.12	98.92	1.01	96.72

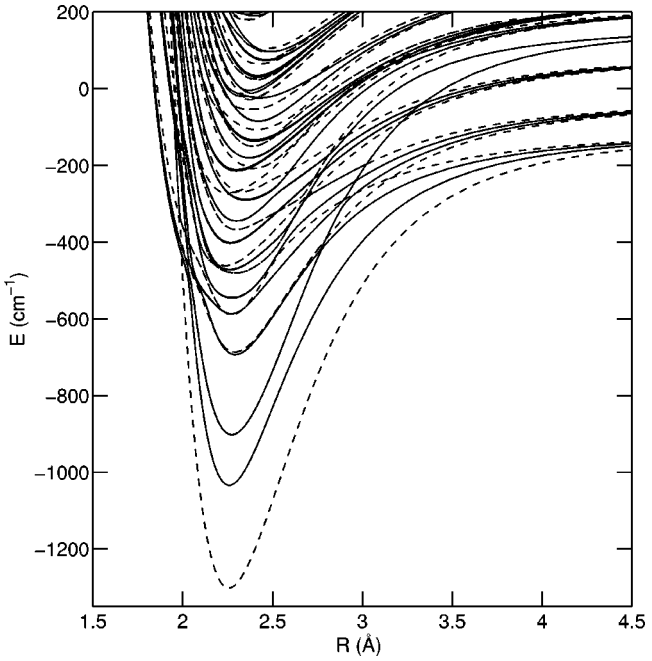

FIG. 1. Energy levels from fixed-R calculations, plotted as functions of R. Closed lines for $|P_R|=\frac{1}{2}, J=\frac{1}{2}$ and dashed lines for $|P_R|=\frac{3}{2}, J=\frac{3}{2}$.

B. Full calculation

Tables III and IV contain the rovibronic energy levels and parity splittings from full-dimensional calculations for $J=\frac{1}{2}, \frac{3}{2}, \frac{5}{2}, \frac{7}{2}, \frac{9}{2}$. The first column indicates the dominant character of the corresponding eigenstate. The label $^{2S+1}K_P$ is commonly used in Renner–Teller systems; the quantum numbers S, $P=P_r$, and $K=K_r$ were defined in Sec. II B.

In the linear triatomic open-shell molecules in which Renner–Teller coupling is mostly studied K is the sum of the electronic orbital angular momentum Λ and the vibrational angular momentum, usually called l, generated by the degenerate bending mode. The quantum number that corresponds most closely to l in the He–HF^+ complex is the quantum number Ω_L defined in the **r** embedding and K is defined in this MF embedding as $K_r=\Lambda+\Omega_L=P_r-\Sigma$. The problem in the BF embedding is that the electronic angular momentum Λ is the projection on the HF^+ axis **r**, the nuclear angular momentum projection Ω_L is not defined, while the total angular momentum projection P_R is defined with respect to the intermolecular vector **R**. Still, we write $K_R=P_R-\Sigma$ also in the BF system. This is physically meaningful because the complex has a linear equilibrium geometry with a rather steep well in which the lower rovibronic states are localized and the vectors **r** and **R** remain nearly parallel. Table V shows a comparison of the main character of the rovibronic states in terms of the quantum numbers for the two embeddings considered. In all cases except a few, in which the character is quite mixed anyway, we find agreement between the assignments of the two embeddings. The population of the dominant $^{2S+1}K_P$ component is systematically higher in the **R** embedding, which shows that this embedding yields the better approximate quantum numbers. This seems in contradiction with our previous observation that the quantum number K is more strictly defined in the **r** embedding, but one should realize that this was a purely formal argument,

TABLE III. Rovibronic energy levels (in cm^{-1}) of parity e in **r** embedding. The assigment in terms of $^{2S+1}K_P$ with $K=K_r$ and $P=P_r$ and the stretch, bend quantum numbers v_s, v_b is explained in the text. States with $|K|=0,1,2,3$ are denoted by Σ, Π, Δ, Φ.

$^{2S+1}K_P(v_s,v_b)$	$J=\frac{1}{2}$	$J=\frac{3}{2}$	$J=\frac{5}{2}$	$J=\frac{7}{2}$	$J=\frac{9}{2}$
$^2\Pi_{3/2}(0,0)$	⋯	−1125.6274	−1121.1001	−1114.7641	−1106.6216
$^2\Pi_{1/2}(0,0)$	−862.7696	−860.0766	−855.5705	−849.2533	−841.1274
$^2\Pi_{3/2}(1,0)$	⋯	−818.1741	−814.0112	−808.1859	−800.7009
$^2\Sigma_{1/2}(0,1)$	−750.4286	−747.9311	−743.6468	−737.5769	−729.7240
$^2\Delta_{5/2}(0,1)$	⋯	⋯	−729.9411	−723.7550	−715.8068
$^2\Pi_{3/2}(2,0)$	⋯	−576.4169	−572.5091	−567.0542	−560.0688
$^2\Sigma_{1/2}(1,1)$	−577.1277	−574.9012	−571.0322	−565.5213	−558.3691
$^2\Pi_{1/2}(0,2)$	−562.9230	−559.9903	−555.3150	−548.9100	−540.7956
$^2\Pi_{3/2}(0,2)$	⋯	−556.4190	−552.1326	−546.1146	−538.3456
$^2\Delta_{5/2}(1,1)$	⋯	⋯	−482.6417	−477.1104	−470.0061
$^2\Pi_{1/2}(1,0)$	−487.2650	−484.9705	−481.0415	−475.4763	−468.2760
$^2\Sigma_{1/2}(0,3)$	−474.7757	−472.2898	−467.9698	−461.8190	−453.8415
$^2\Delta_{3/2}(0,1)$	⋯	−454.5045	−449.9153	−443.4953	−435.2501
$^2\Sigma_{1/2}(0,1)$	−436.7975	−434.3995	−430.1277	−423.9965	−416.0239
$^2\Phi_{7/2}(0,2)$	⋯	⋯	⋯	−415.0390	−407.7367
$^2\Delta_{5/2}(0,3)$	⋯	⋯	−391.2582	−385.9204	−379.0634
$^2\Pi_{3/2}(3,2)$	⋯	−392.7682	−388.2957	−382.2816	−374.9899
$^2\Pi_{3/2}(3,0)$	⋯	−388.3586	−384.6341	−379.2496	−371.9206
$^2\Pi_{1/2}(1,4)$	−383.8626	−381.1165	−376.6832	−370.4884	−362.5129
$^2\Pi_{3/2}(0,4)$	⋯	−370.8265	−366.8738	−361.7200	−355.0922
$^2\Pi_{1/2}(2,2)$	−371.9084	−369.3066	−364.0358	−356.5184	−347.2930
$^2\Sigma_{1/2}(2,3)$	−361.7989	−359.1454	−354.8810	−348.9126	−341.0510
$^2\Pi_{3/2}(1,2)$	⋯	−355.9188	−351.9194	−346.3406	−339.1907
$^2\Sigma_{1/2}(0,5)$	−321.0598	−318.9936	−314.9773	−308.9983	−301.0462
$^2\Delta_{5/2}(1,3)$	⋯	⋯	−304.2796	−298.4314	−291.0522
$^2\Sigma_{1/2}(1,3)$	−303.9462	−302.4868	−299.4022	−294.6780	−288.3062

TABLE IV. Parity splitting $\Delta E = E_f - E_e$ (in cm^{-1}) of the levels in Table III.

$^{2S+1}K_P(v_s,v_b)$	$J=\frac{1}{2}$	$J=\frac{3}{2}$	$J=\frac{5}{2}$	$J=\frac{7}{2}$	$J=\frac{9}{2}$
$^2\Pi_{3/2}(0,0)$	⋯	0.0000	0.0000	0.0001	0.0002
$^2\Pi_{1/2}(0,0)$	0.0567	0.1134	0.1701	0.2267	0.2833
$^2\Pi_{3/2}(1,0)$	⋯	0.0000	0.0000	0.0001	0.0002
$^2\Sigma_{1/2}(0,1)$	0.3675	0.7337	1.0971	1.4565	1.8105
$^2\Delta_{5/2}(0,1)$	⋯	⋯	0.0000	0.0000	0.0000
$^2\Pi_{3/2}(2,0)$	⋯	0.0006	0.0016	0.0023	0.0030
$^2\Sigma_{1/2}(1,1)$	0.4719	0.9376	1.3917	1.8301	2.2484
$^2\Pi_{1/2}(0,2)$	−0.6069	−1.2053	−1.7859	−2.3363	−2.8391
$^2\Pi_{3/2}(0,2)$	⋯	−0.0004	−0.0031	−0.0133	−0.0426
$^2\Delta_{5/2}(1,1)$	⋯	⋯	0.0000	0.0000	0.0000
$^2\Pi_{1/2}(1,0)$	0.2976	0.5844	0.8510	1.0909	1.3006
$^2\Sigma_{1/2}(0,3)$	0.5355	1.0680	1.5937	2.1068	2.6000
$^2\Delta_{3/2}(0,1)$	⋯	−0.0022	−0.0086	−0.0213	−0.0420
$^2\Sigma_{1/2}(0,1)$	0.8638	1.7357	2.6226	3.5299	4.4601
$^2\Phi_{7/2}(0,2)$	⋯	⋯	⋯	0.0000	0.0000
$^2\Delta_{5/2}(0,3)$	⋯	⋯	−0.0023	−0.0065	−0.0070
$^2\Pi_{3/2}(3,2)$	⋯	−0.0006	0.0030	0.0156	0.0283
$^2\Pi_{3/2}(3,0)$	⋯	0.0022	0.0079	0.0184	0.0490
$^2\Pi_{1/2}(1,4)$	−0.6516	−1.2274	−1.6942	−2.0432	−2.2524
$^2\Pi_{3/2}(0,4)$	0.2764	0.2233	0.8807	1.3386	1.6524
$^2\Pi_{1/2}(2,2)$	⋯	0.2969	−0.1394	−0.3734	−0.6122
$^2\Sigma_{1/2}(2,3)$	−0.6501	−1.3329	−2.0817	−2.9202	−3.7046
$^2\Pi_{3/2}(1,2)$	⋯	0.0014	0.0061	0.0158	0.0266
$^2\Sigma_{1/2}(0,5)$	1.6586	3.2800	4.8236	6.2406	7.4659
$^2\Delta_{5/2}(1,3)$	⋯	⋯	0.0014	0.0091	0.0367
$^2\Sigma_{1/2}(1,3)$	1.8674	3.6779	2.6978	2.9431	3.0847

while the assignment of approximate quantum numbers is of more physical nature.

The binding energy D_0 of the complex is 1125.6 cm^{-1} for $J=\frac{3}{2}$, $|P_r|=\frac{3}{2}$, and spectroscopic parity e. Note, for comparison, that the global minimum in this potential at the linear geometry with $R_e=2.24$ Å has well depth $D_e=1631$ cm^{-1}. The analysis of the wave functions using the (BF) **R** embedding shows that the well is sufficiently deep to considerably hinder the rotation of HF^+: basis functions with different j are strongly mixed.

Table III also lists stretch and bend quantum numbers v_s and v_b. The assignment of these quantum numbers was made with the help of the wave functions, some of which are plotted in Figs. 2 and 3. The stretch quantum number v_s is determined by counting the number of nodes in the wave function along the radial coordinate. The bend quantum number v_b is also determined from the number of nodes, but in a slightly more complicated manner. The bending mode of a semirigid triatomic molecule is denoted by v_b^l, where l takes only the values $-v_b, -v_b+2, \ldots, v_b$. Here, the vibrational angular momentum l is equal to $P-\Sigma-\Lambda$. The eigenfunctions of a two-dimensional isotropic harmonic oscillator can be written as $F_{v,l}(q)\exp(il\alpha)$, where q is the amplitude of the bending vibration and α is the phase, and $F_{v,l}(q)$ has $(v-|l|)/2$ nodes. Because l is known, we can count the number of nodes in the wave function along the angular coordinate and deduce the value of v_b.

Comparison of the v_s, $v_b=0,0$ energy levels from the full calculation in Table III with the lower levels from the fixed-R calculation in Tables I and II shows that the stretch zero-point energy of the complex is about 175 cm^{-1}. In the harmonic approximation this would correspond to a stretch frequency of about 350 cm^{-1}. From the energy differences between the $^2\Pi_{3/2}$ levels with $v_s=0,1,2$ and $v_b=0$ we find 308 cm^{-1} for the stretch fundamental frequency and 549 cm^{-1} for the first overtone, indicative of strong anharmonicity. This anharmonicity made it difficult to recognize other stretch progressions. Figure 4 shows an overview of the calculated rovibronic levels with their successive $v_s=1,2,3$ stretch excited states (as far as they could be identified) separated into different columns. Two of the higher diagonal arrows that refer to stretch excitations do not connect states of the same quantum numbers K and P, but one should realize that these approximate quantum numbers are not always well defined. The states concerned are of mixed character and the character may change upon stretch excitation.

The parity splittings of the levels with $J=\frac{1}{2}$ up to $\frac{9}{2}$ presented in Table IV are in reasonable agreement with the results of the fixed-R calculation at 2.26 Å in Tables I and II. The largest splittings occur for the levels with $|P|=\frac{1}{2}$ and these splittings are nicely proportional to $J+\frac{1}{2}$. This simple linear dependence on $J+\frac{1}{2}$ is well known for λ doubling in linear molecules.[12] Here it can be understood by considering the Hamiltonian in Eq. (15) and the parity-adapted basis in Eq. (20). From the latter it follows that the energy difference between functions with e and f parity is caused by a coupling between the basis components $|\Lambda,\Sigma,\Omega,\Omega_L,P_r\rangle$ and $|-\Lambda,-\Sigma,-\Omega,-\Omega_L,-P_r\rangle$. The J-dependent coupling operators in the Hamiltonian of Eq. (15) are the shift operators $\hat{J}_\pm\hat{L}_\pm$ and $\hat{J}_\pm\hat{S}_\pm$. The latter operator indeed gives a first-order splitting between the components with $\Sigma,P_r=\pm\frac{1}{2}$, $\pm\frac{1}{2}$ that is proportional to $\sqrt{[J(J+1)+\frac{1}{4}]}\sqrt{[S(S+1)+\frac{1}{4}]}$

TABLE V. Comparison of the main character (in percent) of the levels in Table III in **R** vs **r** embedding. Quantum numbers P,K are either P_R, K_R or P_r, K_r; the label $^{2S+1}K_P$ corresponds to the latter.

Energy (cm^{-1})	P	K	$K-\Lambda$		**R**-emb	**r**-emb
−1125.6274	$\frac{3}{2}$	1	0	$^2\Pi_{3/2}(0,0)$	99.2	93.2
−862.7696	$\frac{1}{2}$	1	0	$^2\Pi_{1/2}(0,0)$	71.4	70.8
−818.1741	$\frac{3}{2}$	1	0	$^2\Pi_{3/2}(1,0)$	99.1	91.9
−750.4286	$\frac{1}{2}$	0	−1	$^2\Sigma_{1/2}(0,1)$	69.2	68.4
−729.9411	$\frac{5}{2}$	2	1	$^2\Delta_{5/2}(0,1)$	97.9	75.4
−576.4169	$\frac{3}{2}$	1	0	$^2\Pi_{3/2}(2,0)$	96.7	82.2
−577.1277	$\frac{1}{2}$	0	−1	$^2\Sigma_{1/2}(1,1)$	50.9	45.0
	$\frac{1}{2}$	1	0		35.7	34.5
−562.9230	$-\frac{1}{2}$	−1	−2	$^2\Pi_{1/2}(0,2)$	61.7	55.2
−556.4190	$\frac{3}{2}$	1	0	$^2\Pi_{3/2}(0,2)$	89.0	66.9
−482.6417	$\frac{5}{2}$	2	1	$^2\Delta_{5/2}(1,1)$	97.9	69.5
−487.2650	$\frac{1}{2}$	1	0	$^2\Pi_{1/2}(1,0)$	50.3	47.0
	$\frac{1}{2}$	0	−1		46.5	46.5
−474.7757	$\frac{1}{2}$	0	−1	$^2\Sigma_{1/2}(0,3)$	63.2	41.4
	$-\frac{1}{2}$	0	−1		23.6	15.7
	$-\frac{1}{2}$	−1	−2		5.2	27.0
	$\frac{1}{2}$	1	0		8.0	15.0
−454.5045	$\frac{3}{2}$	2	1	$^2\Delta_{3/2}(0,1)$	68.6	30.9
−436.7975	$-\frac{1}{2}$	0	−1	$^2\Sigma_{1/2}(0,1)$	42.2	45.2
	$-\frac{1}{2}$	−1	−2		38.8	10.8
	$\frac{1}{2}$	0	−1		10.2	38.1
−415.0390	$\frac{7}{2}$	3	2	$^2\Phi_{7/2}(0,2)$	93.0	45.1
−391.2582	$\frac{5}{2}$	2	1	$^2\Delta_{5/2}(0,3)$	64.8	31.4
−392.7682	$-\frac{3}{2}$	−2	−3	$^2\Pi_{3/2}(3,2)$	38.1	10.8
	$\frac{3}{2}$	1	0		36.9	30.8
−388.3586	$\frac{3}{2}$	1	0	$^2\Pi_{3/2}(3,0)$	74.4	63.6
−383.8626	$-\frac{1}{2}$	−1	−2	$^2\Pi_{1/2}(1,4)$	61.0	62.1
−370.8265	$\frac{3}{2}$	1	0	$^2\Pi_{3/2}(0,4)$	47.4	19.1
	$\frac{1}{2}$	0	−1		17.3	29.3
	$-\frac{1}{2}$	−1	−2		11.7	22.0
−371.9084	$\frac{1}{2}$	0	−1	$^2\Pi_{1/2}(2,2)$	51.4	38.5
	$-\frac{1}{2}$	−1	−2		30.3	43.2
−361.7989	$-\frac{1}{2}$	−1	−2	$^2\Sigma_{1/2}(2,3)$	50.0	36.3
	$\frac{1}{2}$	0	−1		34.2	48.0
−355.9188	$\frac{3}{2}$	1	0	$^2\Pi_{3/2}(1,2)$	83.5	52.0
−321.0598	$\frac{1}{2}$	0	−1	$^2\Sigma_{1/2}(0,5)$	73.7	58.6
−304.2796	$-\frac{5}{2}$	−3	−4	$^2\Delta_{5/2}(1,3)$	56.6	6.2
	$\frac{5}{2}$	2	1		27.1	14.0
−303.9462	$\frac{1}{2}$	0	−1	$^2\Sigma_{1/2}(1,3)$	74.0	67.6

$=(J+\frac{1}{2})(S+\frac{1}{2})=(J+\frac{1}{2})$. The magnitude of the actual splittings in Table IV is on the order of the end-over-end rotational constant of the complex (see below), rather than the size of the monomer rotational constant B_0 that appears in Eq. (15). This is a consequence of the quenching of the HF^+ monomer rotations in the complex.

From the levels with $J=\frac{1}{2}, \frac{3}{2}, \frac{5}{2}, \frac{7}{2}, \frac{9}{2}$ we extracted rotational constants of the complex. First, we averaged the energies of the e and f states to remove the effect of the parity splitting. We note that the J dependence of the energy levels originates from the term $[\hat{J}^2-2\hat{\mathbf{j}}\cdot\hat{\mathbf{J}}]/(2\mu R^2)$ in the Hamiltonian of Eq. (6). After removal of the parity splitting caused by the J-dependent shift operators the energy contribution of

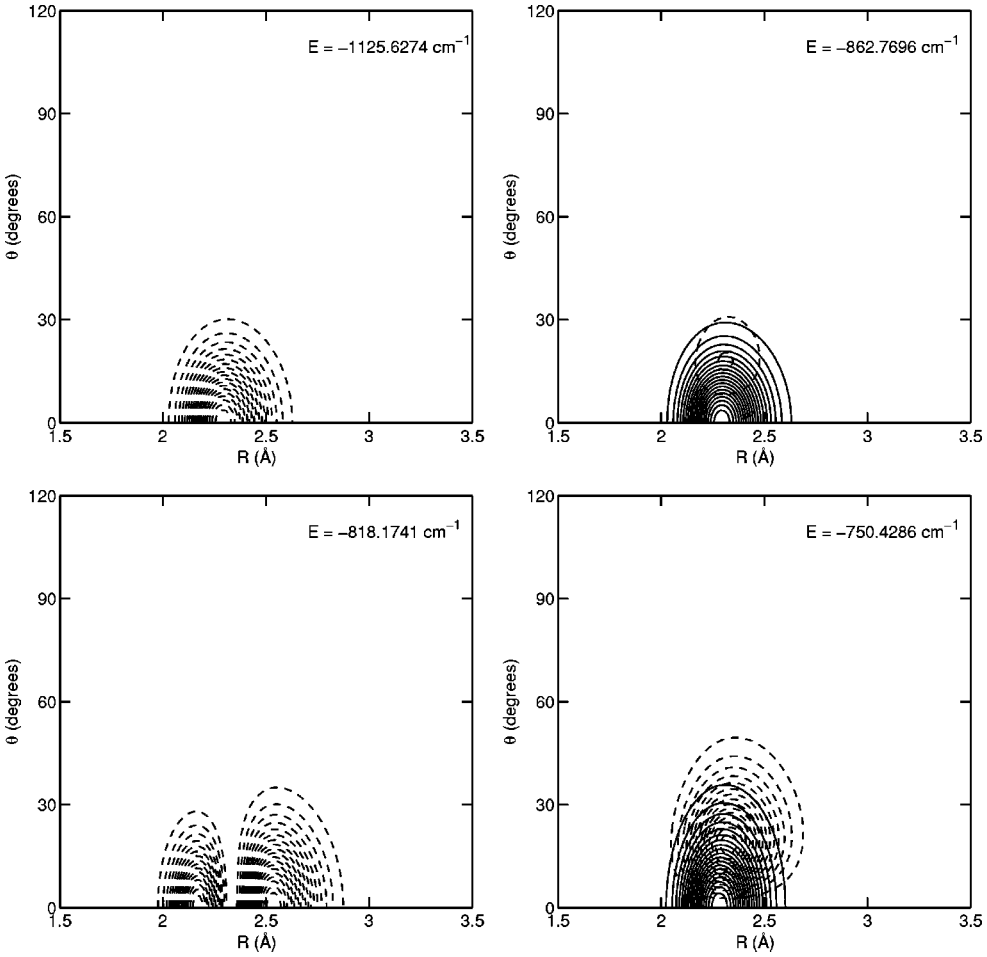

FIG. 2. Density distributions of the lowest four levels from full calculations. The closed and dashed contours are the $|\Omega|=\frac{1}{2}$ and $|\Omega|=\frac{3}{2}$ contributions, respectively. These distributions are the squares of the rovibronic wave functions with $J=|P|$, integrated over all coordinates except R and θ. For the corresponding energy levels and quantum numbers we refer to Table III.

this term is $[J(J+1)-P^2]\langle[2\mu R^2]^{-1}\rangle$. The expectation value $\langle[2\mu R^2]^{-1}\rangle$ is the end-over-end rotational constant of the complex. The band origins E_0, end-over-end rotational constants B, and centrifugal distortion constants D presented in Table VI were obtained by a fit of the levels with $J=\frac{1}{2}$ to $\frac{9}{2}$ for each internal state with the formula

$$E(J,P)=E_0+B[J(J+1)-P^2]-D[J(J+1)-P^2]^2. \quad (21)$$

We observe that a substantial decrease of the end-over-end rotational constant B is caused by one or two quanta of stretch excitation, as might be expected, but that also the combination of one stretch and one bend quantum gives a strong reduction of B.

A similar study of the He–HF$^+$ complex was made earlier by Schmelz and Rosmus[3] on the basis of intermolecular potentials computed by the coupled electron pair approximation. It was already mentioned in Paper I that our potentials are somewhat different from theirs and, in particular, that our binding energy D_e is larger. The rovibronic energy level pattern that they obtain from their potentials is different from ours. The character of the ground state is the same, but the order of the excited states is considerably different. Their spin–orbit splitting $^2\Pi_{1/2}(0,0)-^2\Pi_{3/2}(0,0)$ is 319.6 cm^{-1}, whereas ours is 265.6 cm^{-1}. Their stretch frequency $^2\Pi_{3/2}(1,0)-^2\Pi_{3/2}(0,0)$ is 311.0 cm^{-1}, ours is 307.5 cm^{-1}. The most striking difference occurs for the bend frequency $^2\Sigma_{1/2}(0,1)-^2\Pi_{3/2}(0,0)$ that they find to be 223.2 cm^{-1}, substantially lower than our value of 377.7 cm^{-1}.

Since the intermolecular potential depends strongly on the HF$^+$ bond length, we also computed rovibronic levels with r fixed at the value of 1.0273 Å that corresponds to the global minimum of a full three-dimensional potential surface (see Paper I). The dissociation energy D_e of the complex with respect to He and the HF$^+$ monomer at its equilibrium geometry is increased by 72.3 cm^{-1} by this relaxation of r. The intermolecular zero-point energy increases by 55.4 cm^{-1}, from 505.7 to 561.1 cm^{-1}, making D_0 increase by 16.9 cm^{-1}. The actual increase of D_0 in full three-dimensional calculations is probably larger, however, because the vibrational zero-point energy of HF$^+$ may be lower in the complex. The characteristic excitation energies, 273.1 cm^{-1} for the spin–orbit splitting, 329.4 cm^{-1} for the stretch, and 415.5 cm^{-1} for the bend, are higher than the values calculated for $r=r_e$.

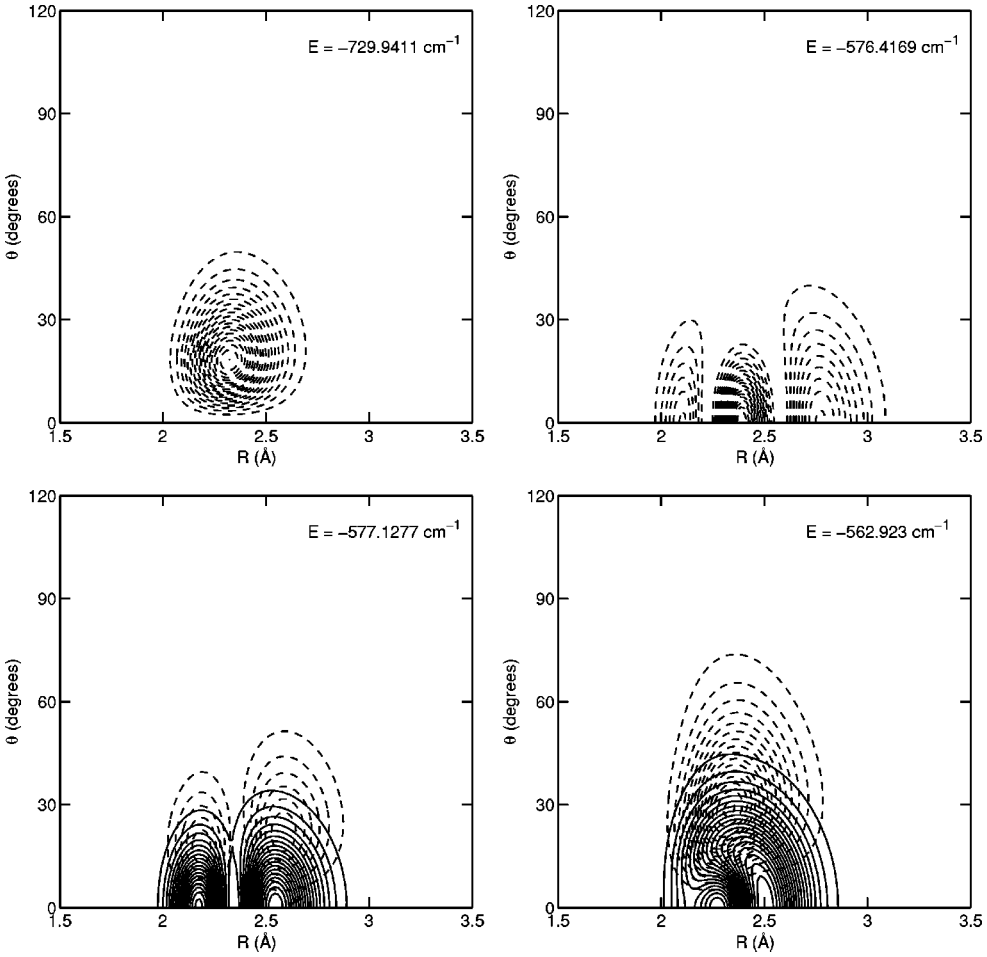

FIG. 3. Density distributions of the next four levels from full calculations. For explanations, see Fig. 2.

C. Renner–Teller effect

The Renner–Teller effect is taken into account in our calculations, because our intermolecular potentials refer to coupled diabatic electronic states and we include all of the relevant electronic and nuclear angular momentum couplings in our Hamiltonian. Our basis can accurately describe the internal (stretch and bend) motions and overall rotation of the $He–HF^+$ complex, even when these internal motions have large amplitudes. Let us now consider explicitly how the Renner–Teller effect becomes manifest in our results. Figure 5 shows the levels calculated for stretch quantum number $v_s=0$, i.e., the leftmost column of Fig. 4. This picture may be directly compared with the energy level diagram of a $^2\Pi$ triatomic linear molecule shown in Herzberg's book,[13] Fig. 8 of Sec. I.2. This diagram correlates the energy levels obtained from a full calculation with the levels obtained when either the Renner–Teller interaction or the spin–orbit coupling are set to zero. Herzberg's ''full'' treatment includes the bending mode only and it defines the Renner–Teller interaction parameter ϵ as the ratio of the harmonic force constants of the coupling or difference potential $V_{1,-1}=(V_{A''}-V_{A'})/2$ and the diagonal or sum potential $2V_{1,1}=V_{A'}+V_{A''}$. The corresponding set of levels from our calculation is shown in the second column of Fig. 5. Note that the bend quantum number v_b in our notation is given in

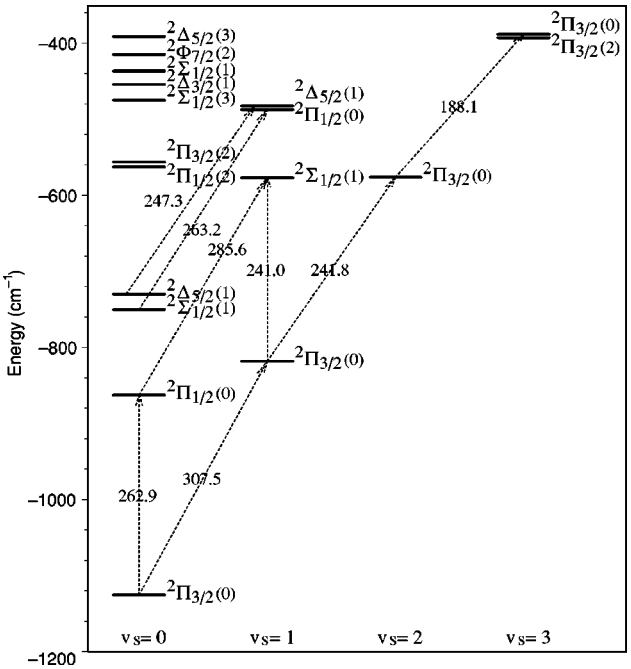

FIG. 4. Rovibronic levels from full calculations. The levels are labeled with the approximate quantum numbers $^{2S+1}K_P(v_b)$, and $|K|=0,1,2,3$ is denoted by Σ,Π,Δ,Φ. The overall angular momentum J is always taken equal to $|P|$.

TABLE VI. Band origins E_0, rotational constants B, and distortion constants D extracted from energy levels with $J=\frac{1}{2},\frac{3}{2},\frac{5}{2},\frac{7}{2},\frac{9}{2}$.

	E_0	B	D
$^2\Pi_{3/2}(0,0)$	−1126.9858	0.9057	0.000 0261
$^2\Pi_{1/2}(0,0)$	−863.1948	0.9072	0.000 0307
$^2\Pi_{3/2}(1,0)$	−819.4233	0.8328	0.000 0323
$^2\Sigma_{1/2}(0,1)$	−750.6916	0.8936	0.000 0358
$^2\Delta_{5/2}(0,1)$	−732.1512	0.8842	0.000 0363
$^2\Pi_{3/2}(2,0)$	−577.5910	0.7832	0.000 1951
$^2\Sigma_{1/2}(1,1)$	−577.3014	0.8198	0.000 0480
$^2\Pi_{1/2}(0,2)$	−563.6658	0.8784	0.000 1176
$^2\Pi_{3/2}(0,2)$	−557.7031	0.8557	−0.000 1637
$^2\Delta_{5/2}(1,1)$	−484.6184	0.7908	0.000 0515

parentheses, while Herzberg's figure shows v_2 on the left-hand side. In Herzberg's figure the levels of the same $|K|$ with the larger $|P|$ are higher than the levels with smaller $|P|$, whereas in our figure the levels with the larger $|P|$ are lower. The reason for this reversed order is that our spin–orbit constant A has a negative value, while Herzberg's is positive. Otherwise, the levels from our calculations follow nicely the pattern of the levels in Herzberg's picture. The gaps between levels with different v_b are smaller in our case, so different v_b manifolds overlap in energy. When we switch off the coupling potential $V_{1,-1}$ we obtain the levels in the first column of Fig. 5. They differ from the levels with $\epsilon=0$ in the first column of Herzberg's picture in that the lower Σ and Δ levels with $v_b=1$ do not become degenerate in our case, and neither do the Π and Φ levels with $v_b=2$. When we set the spin–orbit coupling constant A to zero we produce

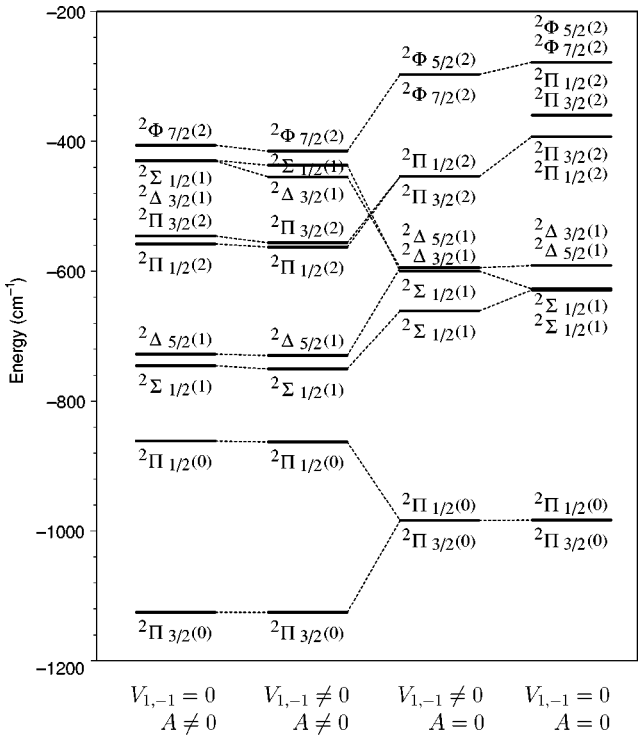

FIG. 5. Correlation diagram showing the dependence of the $v_s=0$ levels on the Renner–Teller interaction potential $V_{1,-1}$ and on the spin–orbit coupling constant A. Labeling of the levels as in Fig. 4.

the levels in the third column of Fig. 5 that are very similar to the levels in the third column of Herzberg's picture, except that the Δ levels with $v_b=1$ are not centered between the Σ levels, but nearly coincide with the upper Σ level. When we switch off both $V_{1,-1}$ and A we produce—cf. the fourth column of Fig. 5—some further degeneracies, but the Δ levels with $v_b=1$ remain higher than the Σ levels, and so do the Φ levels with $v_b=2$ relative to the Π levels. These differences in the first and third columns indicate a fundamental deviation from Herzberg's model, which we will now show to be due to the bending motion being treated as a hindered rotation rather than a harmonic vibration.

This can be understood from an analysis of the matrix elements of the potential $V_{1,1}$ in Eq. (11), but it is easier to consider the example of the HF^+ molecule in a homogeneous electric field of strength F parallel to the SF Z axis. For simplicity we omit the spin, i.e., we put $S=\Sigma=0$ and $\Omega=\Lambda=\pm 1$. When μ is the dipole moment of HF^+ the potential energy can be written as $\hat{V}=-\mu F\cos\theta=-\mu F P_1(\cos\theta)$, with (θ,ϕ) being the SF polar angles of the diatom axis $\mathbf{r}$ and $P_1(\cos\theta)$ the Legendre polynomial P_l with $l=1$. The basis to describe the hindered rotation of HF^+ in this example is obtained from Eq. (9) by omitting the overall rotation functions with quantum numbers J,M_J and depending on the polar angles (β,α) of $\mathbf{R}$. This is equivalent to considering $\mathbf{R}$ (i.e., the direction of the He atom) to be fixed along the SF Z axis (i.e., the field direction). Furthermore, we replace P_R by K because $\Sigma=0$ and get the basis

$$|\Lambda,j,K\rangle=|\Lambda\rangle\sqrt{\frac{2j+1}{4\pi}}D^j_{K,\Lambda}(\phi,\theta,0)^*. \tag{22}$$

The matrix elements of the potential read

$$\langle j',K',\Lambda'|\hat{V}|j,K,\Lambda\rangle = -\mu F\sqrt{(2j'+1)(2j+1)}\times(-1)^{K'-\Lambda'}\begin{pmatrix} j' & 1 & j\\ -K' & 0 & K\end{pmatrix}\begin{pmatrix} j' & 1 & j\\ -\Lambda' & 0 & \Lambda\end{pmatrix}, \tag{23}$$

which is a simplified version of the potential matrix elements with $\Lambda'-\Lambda=0$ in Eq. (11). The kinetic energy operator is given by $\hat{T}=B_0[\hat{\mathbf{j}}-\hat{\mathbf{l}}]^2$, where $\hat{\mathbf{j}}$ is the total angular momentum operator, and $\hat{\mathbf{l}}$ the electronic angular momentum. Only the projection Λ, the eigenvalue of $\hat{l}_z$ with z being the diatom axis $\mathbf{r}$, is a good quantum number and we may therefore omit all of the shift terms with $\hat{l}_\pm$ from the kinetic energy operator. The remaining operator $\hat{T}=B_0[\hat{j}^2+\hat{l}_z^2-2\hat{l}_z\hat{j}_z]$ is diagonal in the basis of Eq. (22), with eigenvalue $B_0[j(j+1)-\Lambda^2]$. Diagonalization of this simple Hamiltonian $\hat{T}+\hat{V}$ in a basis with $j=|\Lambda|,\ldots,j_{\max}$ and plotting the eigenvalues as a function of the field strength F gives the energy level correlation diagram in Fig. 6. Note, in the first place that for sufficiently strong fields the energy levels are very similar to the levels in the rightmost column of Fig. 5. It is clear that the Σ $(K=0)$ and Δ $(|K|=2)$ levels that belong to the first excited "bending" state with $v_b=1$ and $l=\pm 1$ are not degenerate, and neither are the Π $(|K|=1)$ and Φ $(|K|=3)$ levels of the second excited "bending" state with $v_b=2$ and

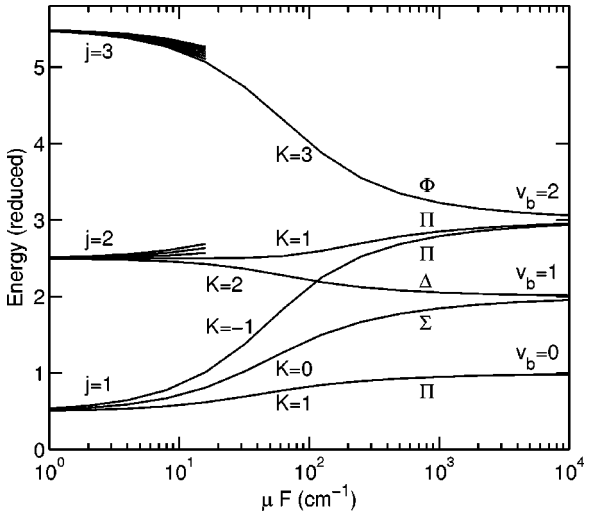

FIG. 6. Energy levels of model HF^+ (with $\Lambda=\pm1$ and $S=0$) in an electric field F as function of the coupling strength μF. The Σ,Π,Δ,Φ labels denote levels with $|K|=0,1,2,3$, while v_b is the "bending" quantum number. The labels K refer to the $\Lambda=+1$ component. The energies are divided by the fundamental "bending" vibration energy defined as $[E_\Sigma(v_b=1)+E_\Delta(v_b=1)]/2-E_\Pi(v_b=0)$.

$l=0,\pm2$. This is related to the finite amplitude of the "bending" motion or, in other words, to the fact that the electronic angular momentum Λ and the total angular momentum K refer to different axes. When the field F becomes stronger, the level pattern becomes more and more similar to that of a harmonic oscillator and the splittings become relatively smaller. In the strong field limit the rotating molecule can hardly bend away from the SF Z axis, the axes Z and z become parallel, and the splitting pattern is similar to Herzberg's.

Also in our calculations on $He–HF^+$ the energy differences between the Δ and Σ levels with $v_b=1$ and between the Φ and Π levels with $v_b=2$ did not disappear, even when we switched off both $V_{1,-1}$ and the spin–orbit coupling. When increasing the steepness of the well at the linear geometry in $V_{1,1}$ we found, also in the full calculations, that these energy differences became relatively small in comparison with the (vibrational) splitting between levels with different v_b. So, in that sense, our results agree with Herzberg's model for the Renner–Teller coupling in a $^2\Pi$ triatomic linear molecule.

IV. CONCLUSION

Without consideration of the spin–orbit coupling the $He–HF^+$ complex has two asymptotically degenerate electronic states that correlate with the $X\,^2\Pi$ ground state of free HF^+. We calculated the bound rovibronic levels of this complex for $J=\frac{1}{2},\frac{3}{2},\frac{5}{2},\frac{7}{2},\frac{9}{2}$ with the use of diabatic intermolecular potentials that couple these states and the inclusion of spin–orbit coupling. The *ab initio* diabatic potential surfaces and their analytic fits are described in Paper I.[1] The calculation of rovibronic levels was performed with basis sets defined in different coordinate frames: a BF frame with the z axis parallel to the vector **R** that points from the center of mass of HF^+ to the He atom, and an MF frame with the z axis parallel to the HF^+ bond axis **r**. We interpreted the character of the rovibronic states by a series of calculations with the $He–HF^+$ distance R fixed at values ranging from 1.5 to 8.5 Å and by analysis of the wave functions. The approximate quantum numbers corresponding to the various angular momentum components with respect to the BF and MF frames were very useful in this analysis.

The intermolecular potential has a rather deep well at the linear $He–HF^+$ geometry, which makes this complex a Renner–Teller system. Renner–Teller effects have mostly been studied for semirigid triatomic and polyatomic linear molecules. Although the $He–HF^+$ complex is much more strongly bound than the neutral He–HF Van der Waals complex, it is considerably less rigid than a "normal" molecule held together by covalent bonds. It was, therefore, interesting to analyze the effects of the Renner–Teller coupling in this system and to look for characteristics due to large amplitude internal motions. We made such an analysis and, indeed, found such features. Finally, we extracted from our results some quantitative data that determine the spectroscopy of this complex: stretch and bend frequencies, spin–orbit splittings, parity splittings, rotational constants, and we compare some of these with the results of a previous theoretical study.

ACKNOWLEDGMENTS

We thank Professor Gilberte Chambaud, Professor Pavel Rosmus, and Dr. Paul E. S. Wormer for valuable discussions and the latter also for critically reading the manuscript. This research has been financially supported by the Council for Chemical Sciences of the Netherlands Organization for Scientific Research (CW-NWO) and by the EU (Theonet II, Grant No. HPRN-CT-1999-00005).

APPENDIX: BASIS TRANSFORMATIONS

Before we discuss the transformation of the different bases, we must derive a relation between the BF and MF frames. For this purpose it is most convenient to take the definition of the BF frame $[\mathbb{R}(\alpha,\beta,\phi)]$ from Sec. II A and to *define* the MF rotation angles by

$$\mathbb{R}(\phi',\theta',\alpha')\equiv\mathbb{R}(\alpha,\beta,\phi)\mathbb{R}(0,\theta,\pi). \tag{A1}$$

Next we verify that this definition is equivalent to the definition of the MF frame given in Sec. II B. Substituting Eq. (A1) into Eq. (13) and using $\mathbb{R}_z(\chi)\mathbf{e}_z=\mathbf{e}_z$ for any angle χ we find

$$r\mathbb{R}(\phi',\theta',\alpha')\mathbf{e}_z=r\mathbb{R}(\alpha,\beta,\phi)\mathbb{R}_y(\theta)\mathbf{e}_z=\mathbf{r}, \tag{A2}$$

where we used Eq. (4) in the last step. To verify Eq. (14) we again substitute Eq. (A1) which gives

$$R\mathbb{R}(\phi',\theta',\alpha')\mathbb{R}_y(\beta')\mathbf{e}_z$$
$$=R\mathbb{R}(\alpha,\beta,\phi)\mathbb{R}(0,\theta,\pi)\mathbb{R}_y(\beta')\mathbf{e}_z=\mathbf{R}, \tag{A3}$$

where we used $\beta'=\theta$, the relation

$$\mathbb{R}_y(\theta)\mathbb{R}_z(\pi)=\mathbb{R}_z(\pi)\mathbb{R}_y(-\theta), \tag{A4}$$

and Eq. (3).

We define electronic basis functions by applying rotation operators of the form $\hat{R}(\alpha,\beta,\gamma)=\hat{R}_z(\alpha)\hat{R}_y(\beta)\hat{R}_z(\gamma)$ to the

wave functions $|\Lambda,S,\Omega\rangle$ with angular momentum projection quantum numbers defined with respect to the SF z axis. This method is particularly convenient for giving a precise definition of open-shell electronic wave functions, also in the case of half-integral spin. In the Appendix of Ref. 14 it was used to define Hund's case (a) basis functions for open-shell diatoms and more details can be found there. Here we extend the technique to define basis functions for open-shell complexes and to derive the transformations between different basis sets. For this purpose we require the rotation operator analogue of Eq. (A1)

$$\hat{R}(\phi',\theta',\alpha')=\hat{R}(\alpha,\beta,\phi)\hat{R}(0,\theta,\pi). \tag{A5}$$

This relation holds for both integral and half-integral angular momentum cases.

Two- and three-angle embedded MF electronic wave functions are defined by

$$|\Lambda,S,\Omega\rangle^{\mathrm{MF},2}\equiv\hat{R}(\phi',\theta',0)|\Lambda,S,\Omega\rangle \tag{A6}$$

and

$$\begin{aligned}|\Lambda,S,\Omega\rangle^{\mathrm{MF}}&\equiv\hat{R}(\phi',\theta',\alpha')|\Lambda,S,\Omega\rangle\\&=\exp(-i\Omega\alpha')|\Lambda,S,\Omega\rangle^{\mathrm{MF},2}.\end{aligned} \tag{A7}$$

Electronic wave functions defined with respect to the (three-angle embedded) BF frame are given by

$$|\Lambda,S,\Omega\rangle^{\mathrm{BF}}\equiv\hat{R}(\alpha,\beta,\phi)\hat{R}(0,\theta,0)|\Lambda,S,\Omega\rangle, \tag{A8}$$

where we use the BF label, even though these functions are quantized with respect to the HF$^+$ axis, just as the MF functions. This can be readily verified since the operator relation in Eq. (A5) yields

$$|\Lambda,S,\Omega\rangle^{\mathrm{BF}}=\exp(i\Omega\pi)|\Lambda,S,\Omega\rangle^{\mathrm{MF}}. \tag{A9}$$

In Ref. 9 a basis for the He–HF$^+$($X\,^2\Pi$) complex in SF coordinates

$$\begin{aligned}&|n,\Lambda,S,\Omega,j,L;J,M_J\rangle\\&=|n\rangle|\Lambda,S,\Omega\rangle^{\mathrm{MF},2}\left[\frac{2j+1}{4\pi}\right]^{1/2}\sum_{m,M_L}D^{(j)}_{m,\Omega}(\phi',\theta',0)^*\\&\quad\times Y_{L,M_L}(\beta,\alpha)\langle j,m;L,M_L|J,M_J\rangle\end{aligned} \tag{A10}$$

was obtained by coupling the HF$^+$ monomer functions with total angular momentum j and the spherical harmonics $Y_{L,M_L}(\beta,\alpha)$ by means of the Clebsch–Gordan coefficients $\langle j,m;L,M_L|J,M_J\rangle$.[11] The two-angle embedded electronic wave function may be replaced by $|\Lambda,S,\Omega\rangle^{\mathrm{MF}}$ if simultaneously the third argument (0) of the function $D^{(j)}_{m,\Omega}$ is set to α'. By a straightforward extension of the definition of the case (a) basis in Ref. 14 we define a MF basis for the complex as

$$\begin{aligned}&|n,\Lambda,S,\Omega,L,\Omega_L,P_r;J,M_J\rangle\\&=|n\rangle\left[\frac{2J+1}{4\pi}\right]^{1/2}D^{(J)}_{M_J,P_r}(\phi',\theta',0)^*\\&\quad\times\hat{R}(\phi',\theta',0)[Y_{L,\Omega_L}(\beta,\alpha)|\Lambda,S,\Omega\rangle],\end{aligned} \tag{A11}$$

where the rotation operator acts on the electronic coordinates, as well as on (β,α). With the use of Eq. (A7) and the relation $P_r=\Omega+\Omega_L$ we obtain the MF basis in Eq. (17).

Analogously we define the **R** embedded (BF) basis

$$\begin{aligned}&|n,\Lambda,S,\Omega,j,P_R;J,M_J\rangle\\&=|n\rangle\frac{[(2J+1)(2j+1)]^{1/2}}{4\pi}D^{(J)}_{M_J,P_R}(\alpha,\beta,0)^*\\&\quad\times\hat{R}(\alpha,\beta,0)[D^{(j)}_{P_R,\Omega}(\phi',\theta',0)^*\\&\quad\times\hat{R}(\phi',\theta',0)|\Lambda,S,\Omega\rangle].\end{aligned} \tag{A12}$$

Acting with the rotation operators on the electronic and nuclear coordinates and using the BF electronic wave functions from Eq. (A8) we obtain Eq. (9).

The elements of the unitary matrix that transforms the coupled SF basis into the MF basis are the overlap integrals

$$\begin{aligned}&T^{(\Omega,L,J)}_{\Omega_L,j}\\&=\langle n,\Lambda,S,\Omega,L,\Omega_L,P_r;J,M_J|n,\Lambda,S,\Omega,j,L;J,M_J\rangle\end{aligned} \tag{A13}$$

that can be evaluated by integration over nuclear and electronic coordinates after substitution of Eqs. (17) and (A10). Upon switching to the three-angle MF electronic wave functions introduced in Eq. (A7) the electronic integral becomes simply ${}^{\mathrm{MF}}\langle\Lambda,S,\Omega|\Lambda,S,\Omega\rangle^{\mathrm{MF}}=1$. The integration over the nuclear coordinates is performed most easily in the MF coordinates θ', ϕ', β', and α'. We substitute

$$Y_{L,M_L}(\beta,\alpha)=\hat{R}^{-1}(\phi',\theta',0)Y_{L,M_L}(\beta',\alpha') \tag{A14}$$

$$=\sum_{M_L'}Y_{L,M_L'}(\beta',\alpha')D^{L}_{M_L,M_L'}(\phi',\theta',0)^*. \tag{A15}$$

After integration over α' only the term with $M_L'=\Omega_L$ survives, which allows us to integrate over β'. Upon introduction of a dummy third angle χ via $1/2\pi\int_0^{2\pi}d\chi\exp[i(P_r-\Omega-\Omega_L)\chi]=1$ the remaining integral of the product of three D matrices over ϕ' and θ' becomes a standard integral.[8] The result is a product of two Clebsch–Gordan coefficients. Finally the summation over m and M_L may be performed by using the orthogonality relation of Clebsch–Gordan coefficients[11] and we obtain

$$T^{(\Omega,L,J)}_{\Omega_L,j}=\left[\frac{2j+1}{2J+1}\right]^{1/2}\langle j,\Omega,L,\Omega_L|J,P_r\rangle. \tag{A16}$$

The elements of the matrix that transforms the SF basis into the BF basis can be evaluated similarly

$$T^{(j,J)}_{P_R,L}=\langle n,\Lambda,S,\Omega,j,P_R;J,M_J|n,\Lambda,S,\Omega,j,L;J,M_J\rangle. \tag{A17}$$

Here the electronic integral yields ${}^{\mathrm{BF}}\langle\Lambda,S,\Omega|\Lambda,S,\Omega\rangle^{\mathrm{MF}}=\exp(-i\Omega\pi)$. The nuclear integral is most easily evaluated in BF coordinates, which requires the substitution

$$\begin{aligned}&D^{(j)}_{m,\Omega}(\phi',\theta',\alpha')^*\\&=\sum_{\Omega'}D^{(j)}_{m,\Omega'}(\alpha,\beta,\phi)^*D^{(j)}_{\Omega',\Omega}(0,\theta,\pi)^*.\end{aligned} \tag{A18}$$

This relation is simply a representation of the operator relation in Eq. (A5). After integration over ϕ we find that only the term with $\Omega' = P_R$ survives. The argument π in the last D-matrix cancels the factor from the electronic integral and the remaining integrals are readily performed using expressions from Ref. 8. Again using the orthogonality of the Clebsch–Gordan coefficients in the last step, we find

$$T^{(j,J)}_{P_R,L} = \left[\frac{2L+1}{2J+1}\right]^{1/2} \langle j, P_R, L, 0 | J, P_R \rangle. \tag{A19}$$

[1] V. F. Lotrich, P. E. S. Wormer, and A. van der Avoird, J. Chem. Phys. **120**, 93 (2004), preceding paper.
[2] V. F. Lotrich and A. van der Avoird, J. Chem. Phys. **118**, 1110 (2003).
[3] T. Schmelz and P. Rosmus, Chem. Phys. Lett. **220**, 117 (1994).
[4] A. van der Avoird, P. E. S. Wormer, and R. Moszynski, Chem. Rev. (Washington, D.C.) **94**, 1931 (1994).
[5] P. E. S. Wormer and A. van der Avoird, Chem. Rev. (Washington, D.C.) **100**, 4109 (2000).
[6] M.-L. Dubernet, D. Flower, and J. M. Hutson, J. Chem. Phys. **94**, 7602 (1991).
[7] K. P. Huber and G. Herzberg, *Molecular Spectra and Molecular Structure. IV. Constants of Diatomic Molecules* (Van Nostrand–Reinhold, New York, 1979).
[8] L. C. Biedenharn and J. D. Louck, *Angular Momentum in Quantum Physics*, Encyclopedia of Mathematics, Vol. 8 (Addison-Wesley, Reading, MA, 1981).
[9] W. B. Zeimen, G. C. Groenenboom, and A. van der Avoird, J. Chem. Phys. **119**, 131 (2003).
[10] J. Tennyson and B. T. Sutcliffe, J. Chem. Phys. **77**, 4061 (1982).
[11] D. M. Brink and G. R. Satchler, *Angular Momentum*, 3rd ed. (Clarendon, Oxford, 1993).
[12] H. Lefebvre-Brion and R. W. Field, *Perturbations in the Spectra of Diatomic Molecules* (Academic, New York, 1986).
[13] G. Herzberg, *Molecular Spectra and Molecular Structure*, Electronic Spectra and Electronic Structure of Polyatomic Molecules, Vol. 3 (Van Nostrand, New York, 1950).
[14] M. C. G. N. van Vroonhoven and G. C. Groenenboom, J. Chem. Phys. **117**, 5240 (2002).